AGU PUBLICATIONS

JGR

Journal of Geophysical Research: Oceans

RESEARCH ARTICLE

10.1002/2016JC011742

**Key Points:**
- The spatiotemporal pressure field induced by acoustic-gravity waves from submarine earthquakes is presented
- Acoustic-gravity modes may induce comparable pressure at different water depths
- The total pressure field depends on the presence of a leading acoustic-gravity wave mode, not necessarily the first

**Correspondence to:**
Tiago C. A. Oliveira,
toliveira@whoi.edu

**Citation:**
C. A. Oliveira, T., and U. Kadri (2016), Pressure field induced in the water column by acoustic-gravity waves generated from sea bottom motion, *J. Geophys. Res. Oceans, 121*, doi:10.1002/2016JC011742.

Received 19 FEB 2016
Accepted 22 SEP 2016
Accepted article online 28 SEP 2016



# Pressure field induced in the water column by acoustic-gravity waves generated from sea bottom motion

**Tiago C. A. Oliveira[1,2] and Usama Kadri[3,4]**

[1]Applied Ocean Physics and Engineering Department, Woods Hole Oceanographic Institution, Woods Hole, MA, USA, [2]The Hatter Department of Marine Technologies, University of Haifa, Halfa, Israel, [3]School of Mathematics, Cardiff University, Cardiff, CF24 4AG, UK, [4]Department of Mathematics, Massachusetts Institute of Technology, Cambridge, MA, USA

**Abstract** An uplift of the ocean bottom caused by a submarine earthquake can trigger acoustic-gravity waves that travel at near the speed of sound in water and thus may act as early tsunami precursors. We study the spatiotemporal evolution of the pressure field induced by acoustic-gravity modes during submarine earthquakes, analytically. We show that these modes may all induce comparable temporal variations in pressure at different water depths in regions far from the epicenter, though the pressure field depends on the presence of a leading acoustic-gravity wave mode. Practically, this can assist in the implementation of an early tsunami detection system by identifying the pressure and frequency ranges of measurement equipment and appropriate installation locations.

## 1. Introduction

Although the majority of water wave research consider the ocean as an incompressible medium, the slight compressibility of the ocean water is important in the process of tsunami generation [*Miyoshi*, 1954; *Yamamoto*, 1982; *Nosov*, 1999; *Stiassnie*, 2010]. If the compressibility of the ocean is considered, a disturbance at the ocean floor may generate Acoustic-Gravity Waves (AGWs), progressive compression-type waves that travel at near the speed of sound in water. Recent studies indicate that as AGWs travel they leave measurable bottom pressure signatures that can act as tsunami precursors [*Stiassnie*, 2010; *Chierici et al*., 2010; *Kadri and Stiassnie*, 2012; *Hendin and Stiassnie*, 2013; *Cecioni et al*., 2014; *Abdolali et al*., 2015a]. In this regard, it is anticipated that such utilization of AGWs would enhance current early tsunami detection systems.

In addition to submarine earthquakes, AGWs can be generated by nonlinear interaction of gravity waves of comparable frequencies [*Longuet-Higgins*, 1950; *Kibblewhite and Ewans*, 1985; *Farrell and Munk*, 2010; *Kadri and Stiassnie*, 2013; *Kadri*, 2015; *Kadri and Akylas*, 2016]; space-time localized pressure on the ocean surface induced by storms [*Renzi and Dias*, 2014], submarine landslides [*Synolakis et al*., 2002], ice-quakes [*Kadri*, 2016b], and other sources not yet studied in detail (e.g., submarine volcanoes and landslides).

AGWs generated by an uplift of the ocean bottom have some features that distinct them from AGWs generated by other sources. In fact, an uplift of the ocean bottom can produce many wave modes of three different types. Most of these modes are nonpropagating (evanescent), and their importance is confined to the source zone. A gravity wave mode (tsunami) and AGW mode are also generated. The latter propagate away from the source, and can travel to great distances [*Stiassnie*, 2010; *Kadri and Stiassnie*, 2012]. Each incident AGW mode propagates at a specific frequency, which decays exponentially in time [*Stiassnie*, 2010].

A submarine earthquake also generates seismic waves that propagate within the solid Earth. These waves are responsible for the generation of oceanic Rayleigh waves, leaking *P* wave modes and acoustic organ-pipe waves [*Maeda and Furumura*, 2013; *Kozdon and Dunham*, 2014]. Therefore, the water pressure field at a certain distance from the epicenter of a submarine earthquake must be considered as the sum of the contribution of multiple wave types. However, each of these waves has different propagation characteristics and dependency on the seismological source. Therefore, it is essential to study the behavior of each propagating wave mode, individually, in order to develop an accurate early tsunami detection system. Propagating AGW modes generated by a submarine earthquake are the focus of this work.

Due to the complexity of the physical processes of the seismic source, describing the bottom motion becomes rather challenging [*Banerjee et al*., 2005; *Ammon et al*., 2005; *Pietrzak et al*., 2007; *Grilli et al*., 2008], and simulating the dynamical processes in the tsunami and AGWs source becomes complicated [*Nosov and Kolesov*, 2007]. Notwithstanding, it is known that properties of AGWs depend on rupture model parameters such as the vertical and lateral extent and duration of bottom motion [*Yamamoto*, 1982; *Nosov*, 1999; *Chierici et al*., 2010; *Stiassnie*, 2010; *Hendin and Stiassnie*, 2013]. Current AGW models consider simple geometries and displacements of bottom motions. Example of these motions include rectangular disturbances with constant [*Nosov*, 1999; *Chierici et al*., 2010; *Stiassnie*, 2010; *Hendin and Stiassnie*, 2013] or variable velocities [*Yamamoto*, 1982; *Nosov and Kolesov*, 2007; *Abdolali et al*., 2015a] in the two-dimensional problem, or circular disturbances with constant velocities in the three-dimensional case [*Hendin and Stiassnie*, 2013].

In this work, we study the spatiotemporal evolution of the pressure field induced by AGWs in order to prepare the ground for the implementation of an early tsunami detection system. The fundamental AGW modes generated by a submarine earthquake are calculated based on the analytical expression for wave radiation by a bottom displacement proposed by *Stiassnie* [2010]. Using an example based on the 2004 Indian Ocean earthquake, we consider the first five AGW modes and analyze the temporal variations in pressure at different water depths in regions far from the epicenter. Special emphasis is put on the analysis of the role of the leading AGW in the water pressure field. The analytical solution by *Stiassnie* [2010] is valid for constant water depth at large distances from the epicenter. This solution does not consider damping behavior, porous sedimentary layers, and elasticity at the bottom as well as variations of sound speed along the water column. In addition, low frequency AGWs cannot pass edges and reach shallower areas if they have not damped before due to dissipation at the sea bottom [*Nosov and Kolesov*, 2007; *Abdolali et al*., 2015b]. However, *Sammarco et al*. [2013] observed that the analytical solution by *Stiassnie* [2010], for cases under the limits of its application, is in a good agreement with the full three-dimensional model and depth-integrated model (hyperbolic mild-slope equation) of the weakly compressible, inviscid and irrotational fluid equations. Therefore, the model by *Stiassnie* [2010] presents a fast way to estimate the characteristics of AGWs.

It is worth noting that while in general sea bottom motion generates AGWs, not all the sea bottom motion generates dangerous tsunamis, and the link between the detection of AGWs and the actual generation of a noticeable tsunami still presents important scientific challenges.

This paper is composed of five sections. A background on the 2004 Indian Ocean earthquake and the main properties of AGWs are given in section 2. Taking as example the 2004 Indian Ocean earthquake, the role of the leading AGW mode is discussed in section 3. Next, we present the pressure field induced by the AGWs triggered by the earthquake. Finally, concluding remarks are given in section 5.

## 2. Background

Over 225,000 people found their death along the Indian Ocean coasts by the tsunami generated by the 26 December 2004 Indian Ocean earthquake. A moment magnitude ($M_w$) 9.0–9.3 [*Kanamori*, 2006] ruptured about 1300 km segment of the plate boundary fault in a complex sequence of rapid and slow slip episodes [*Banerjee et al*., 2005; *Ammon et al*., 2005; *Heki et al*., 2006]. Seismic inversion models indicated that the earthquake initiated slowly, with small slip but grew rapidly after about 40–60 s and lasted for more than 1000 s [*Ammon et al*., 2005; *de Groot-Hedlin*, 2005]. The earthquake resulted from an arched rupture zone, with a minimum of 34 separate subzones and in some segments an uplift of the ocean bottom reaching up to 5 m was estimated [*Ammon et al*., 2005]. Due to the magnitude of the earthquake, a destructive tsunami arrived to different coastlines of Indian Ocean countries. It took the tsunami 34 min to reach Banda Aceh in Indonesia (250 km), 1 h 40 min to Thailand (700 km), 2 h to Sri Lanka (1200 km), 3 h 25 min to Maldives (2300 km), and 7 h to Somalia (5000 km).

*Yamamoto* [1982], *Nosov* [1999], *Chierici et al*. [2010], *Stiassnie* [2010], and *Hendin and Stiassnie* [2013] show theoretically how an ocean bottom uplift can simultaneously generate a tsunami and AGWs. They demonstrate that the magnitudes of a tsunami and AGWs depend on the same parameters such as the water depth, vertical displacement, and duration and length of the bottom uplift. Many aspects of AGWs have been studied recently [*Eyov et al*., 2013; *Kadri and Stiassnie*, 2013; *Kadri*, 2014; *Abdolali et al*., 2015b; *Kadri*, 2015, 2016a; *Kadri and Akylas*, 2016]. However, some overlooked AGW key features are introduced here.

Let us consider the ocean an ideal compressible homogeneous fluid. Then, for each frequency $\omega$ and constant water depth $h$, there are $m$ progressive wave modes with wavenumbers $k_n$, $n=0,1,2,\ldots,m$. According to *Kadri and Stiassnie* [2012], $m$ is given by the nearest integer smaller than $(\omega h/\pi c+1/2)$, where $c$ is the speed of sound in water, assumed constant. The first wavenumber $k_0$ is real and it represents the surface gravity wave. The modes, $n=1,2,3,\ldots,m$, are known as AGWs. Consider $\mu_0$ and $\mu_n$ as the solutions of the dispersion relation such that

$$\omega^2=g\mu_0\tanh(\mu_0 h);\quad \omega^2=-g\mu_n\tan(\mu_n h),\quad n=1,2,\ldots. \tag{1}$$

the wavenumbers are real and positive, and given by

$$k_0=(k_s^2+\mu_0^2)^{1/2};\quad k_n=(k_s^2-\mu_n^2)^{1/2},\quad n=1,2,\ldots.,m;\quad k_s>\mu_n \tag{2}$$

where $k_s$ is the wavenumber of sound waves in an unbounded medium ($k_s=\omega/c$) and $g$ is the acceleration due to gravity.

Consider the two-dimensional problem of a progressive AGW mode in an ideal compressible ocean, where $x$ is the direction of the propagating wave and $z$ is the vertically upward. Then, considering the velocity potential [*Kadri*, 2015] and making use of the dispersion relation from equation (1), the dynamic pressure, $p_d$, induced by an AGW is given by

$$p_d=g\rho\frac{H_n}{2}\frac{\cosh(\mu_n(z+h))}{\cosh(\mu_n h)}\cos(k_n x-\omega t) \tag{3}$$

where $\rho$ is the density of the fluid, $H_n$ is the wave height of the $n$th mode, and $t$ is the time.

For the surface wave case, the dynamic pressure decreases exponentially with depth. However, for AGW, the dynamic pressure is periodic with depth. This behavior corresponds to the horizontal water particle displacement and velocity [*Kadri*, 2014] with $(2n-1)/4$ wavelengths fitting the depth for the $n$th AGW mode. Consequently, each AGW mode induces $I$ nodes (including one at the surface) at a distance $Z\leq h$ from the water surface

$$Z_n^I=\frac{2(n-I)h}{2n-1},\quad I=1,2,\ldots,n\quad . \tag{4}$$

## 3. The Role of the Leading AGW Mode

Consider the first five incident AGW modes generated by a bottom uplift $\zeta_0=1$ m, lateral extent of the bottom uplift $b=40$ km, a duration of the bottom motion $\tau=10$ s, propagating in a rigid bottom ocean at a constant water depth $h=4$ km, constant water density $\rho=1000$ kg/m$^3$ and constant speed of sound $c=1500$ m/s. At 50 and 1000 km from the epicenter, AGWs arrive 0.56 and 11.11 min after the eruption, respectively. At 50 km from the epicenter, the first five modes become evanescent at 4.83, 13.98, 23.33, 32.50, and 41.75 min after the eruption, respectively (see Figure 1a). At 1000 km from the epicenter, the evanescent times increase to 93.58, 278.17, 463.17, 648.17, and 833.33 minutes for the first five modes, respectively (see Figure 1b). The closer the detection system to the epicenter, the shorter the action time of each mode becomes. The frequency drops exponentially after the arrival of AGWs and until the moment corresponding mode becomes evanescent (equation (A5)).

Figure 2 shows the spatiotemporal evolution of the envelope of the dynamic bottom pressure, $P_b$ (equation (A2)), induced by the first AGW mode. Between 50 and 1000 km from the earthquake epicenter, an absolute maximum in the bottom pressure is induced by each mode just after the arrival of AGWs. Local maxima in the bottom pressure induced by each mode are observed just before the corresponding mode becomes evanescent. The first AGW mode at its arrival reaches a maximum dynamic bottom pressure of about $5.0\times10^4$ or $1.0\times10^4$ Pa at 50 or 1000 km from the epicenter, respectively. The temporal evolution pattern of the bottom pressure is similar between 50 and 1000 km from the epicenter. However, and as expected, closer to the source the magnitude of the bottom pressure is higher though the action time of the first mode is shorter.

The time that takes each AGW mode to become evanescent depends on the water depth and duration of the bottom uplift movement. In Figure 3, we present the action time for the first AGW mode considering

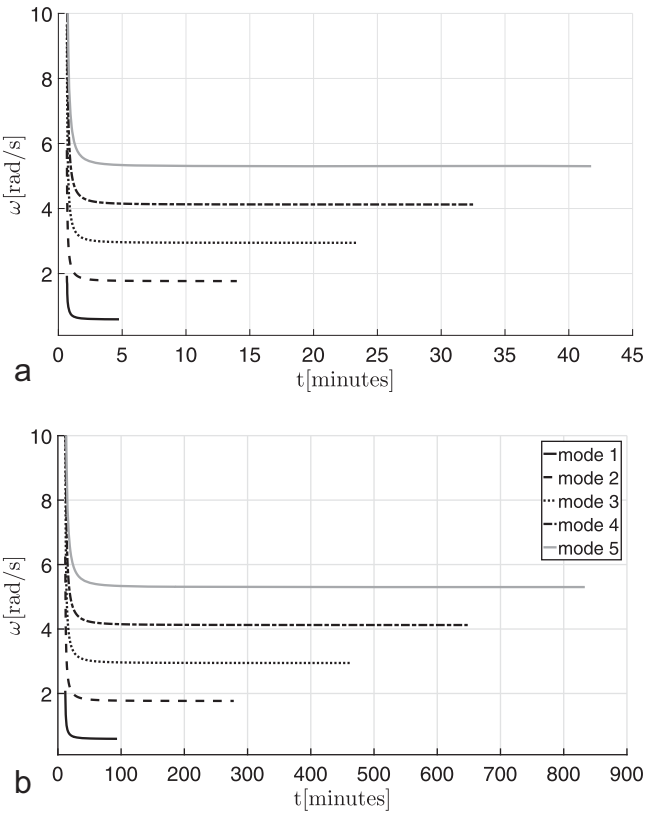


**Figure 1.** Temporal evolution of AGW frequency $\omega$ at (a) $x = 50$ km and (b) $x = 1000$ km. Each line represents one of the first five AGW modes until it becomes evanescent. The simulation considers a vertical bottom uplift $\tau = 10$ s and speed of sound $c = 1500$ m/s.

the cases of an ocean of 2, 3, and 5 km water depth. For each considered water depth, an uplift of 10 and 1000 s is considered. At 50 km from the epicenter, the first AGW mode becomes evanescent between 4.33 and 15.06 min after the eruption, corresponding to an uplift of 10 and 1000 s in a 5 and 2 km water depth, all respectively. At 1000 km from the epicenter, AGWs arrive 11.11 min after the eruption and the first mode becomes evanescent at [131.72–139.95], [107.72–115.95], and [83.89–92.11] min after the eruption for 2, 3, and 5 km water depth, respectively. Together with the bottom pressure, these indicate that the analysis of the first AGW at 50 or 1000 km from the epicenter is both relevant for detecting the tsunami arrival to Thailand, Sri Lanka, Maldives, and Somalia in the 2004 Indian Ocean case.

In order to employ AGWs in an early tsunami detection system, it is crucial to identify the frequency band width of the leading mode. Each mode vanishes at a cutoff frequency $f=(2n-1)c/4h$. So that the frequency decreases as the water depth increases. At 1 km water depth, the frequency of the first mode is 0.375 Hz, whereas for water deeper than 4 km, the frequency is below 0.094 Hz. For the fifth mode and depths between 1 and 7 km, the frequency range is 0.482–3.375 Hz. At these depths, the frequency of the twentieth mode varies from 2.089 to 14.625 Hz.

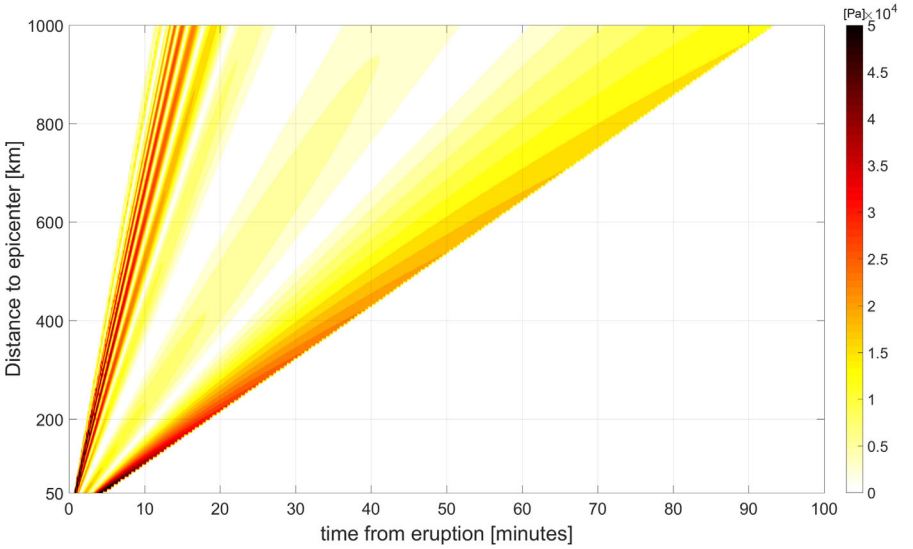


**Figure 2.** Envelope of the dynamic bottom pressure, $P_b$, induced by the first AGW. At $x = 50$ and 1000 km the bottom pressure induced by the first AGW mode can be detected between $t = 0.56 - 4.83$ and $11.11 - 93.58$ min, respectively. The simulation considers a vertical bottom uplift $\tau = 10$ s, lateral extent of the bottom uplift $b = 40$ km and speed of sound $c = 1500$ m/s.

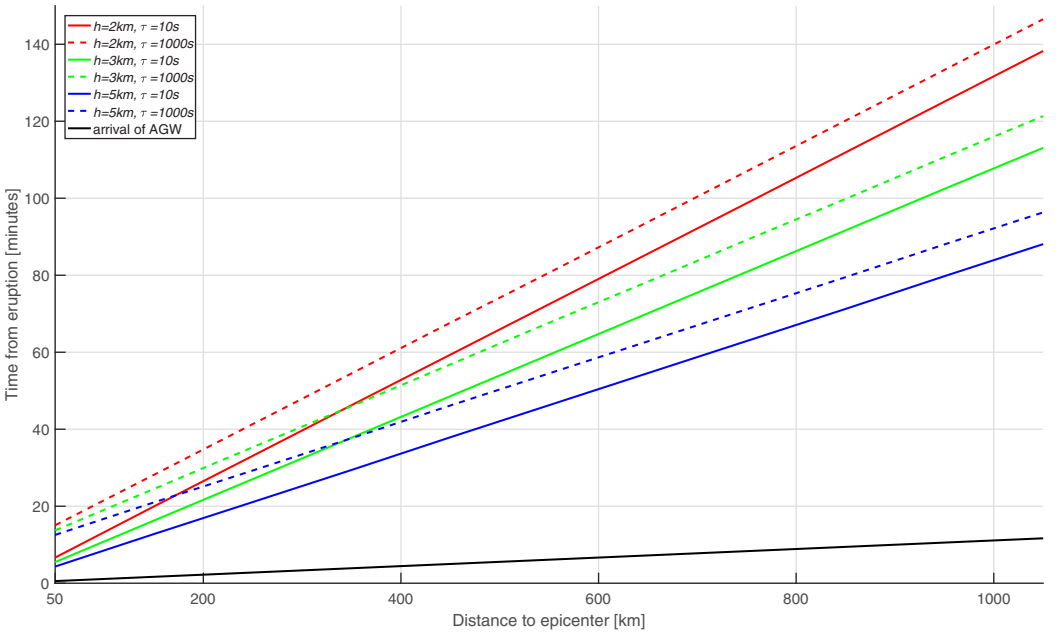


**Figure 3.** Time that takes the first AGW mode generated by a submarine earthquake to become evanescent as function of the distance to the epicenter considering an ocean of 2, 3, and 5 km deep. For each water depth (represented by same color) a bottom uplift of 1000 and 10 s are considered. The critical evanescent time increases with the distance to the epicenter and the duration of the bottom uplift and decreases with the water depth.

## 4. Pressure Field

Calculation of AGWs indicates comparable maximum and minimum pressure values between 1 km water depth and the bottom. Maximum dynamic pressure of $0.8 \times 10^4$ to $1.2 \times 10^4$ Pa could be observed after the arrival of AGWs at 1000 km from the epicenter (equation (3)). The temporal evolution of the dynamic pressure field at 1000 km from the epicenter is given in Figure 4 for six different time intervals. Each time interval represents a different superposition of AGW modes corresponding to the arrival of AGWs and first to fifth mode as the leading mode. Since the problem is linear, each incident mode is solved separately and then all solutions are superposed. The wave heights in equation (3) are calculated as the difference between the maximum and the minimum free surface level given by equation (A1). Each mode is only computed for the period of time between the arriving AGWs and the corresponding evanescent critical time. After the first mode vanishes (Figures 4b–4f) more nodes start to be observed in the water column (in addition to the one at the surface). Consequently, at some depths, no significant temporal pressure variations occur. As an AGW mode becomes evanescent energy is transferred to the next higher modes and the main pattern of the pressure field changes. It is also noted that the first five AGW modes induce comparable temporal pressure variations at different water depths, and thus might all need to be considered.

## 5. Concluding Remarks

Our analysis and simulations shed light on the spatiotemporal evolution of the pressure field induced by AGW that radiate during submarine earthquakes. We consider the first five AGW modes generated by a bottom uplift and show that they may all induce comparable temporal variations in pressure at different water depths in regions far from the epicenter.

Each AGW mode becomes evanescent at a different critical time, at which energy is transferred to the next higher modes. Consequently, the main pattern of the pressure field changes with the leading mode. Based on an example from the 2004 Indian Ocean earthquake, we conclude that at 50 km from the epicenter, where AGWs should have arrived 0.56 min after the eruption, the first AGW mode should have become evanescent between 4.33 and 15.06 min after the eruption. These evanescent values depend on the uplift duration and water depth considered as the 2004 Indian Ocean earthquake was a complex sequence of rapid

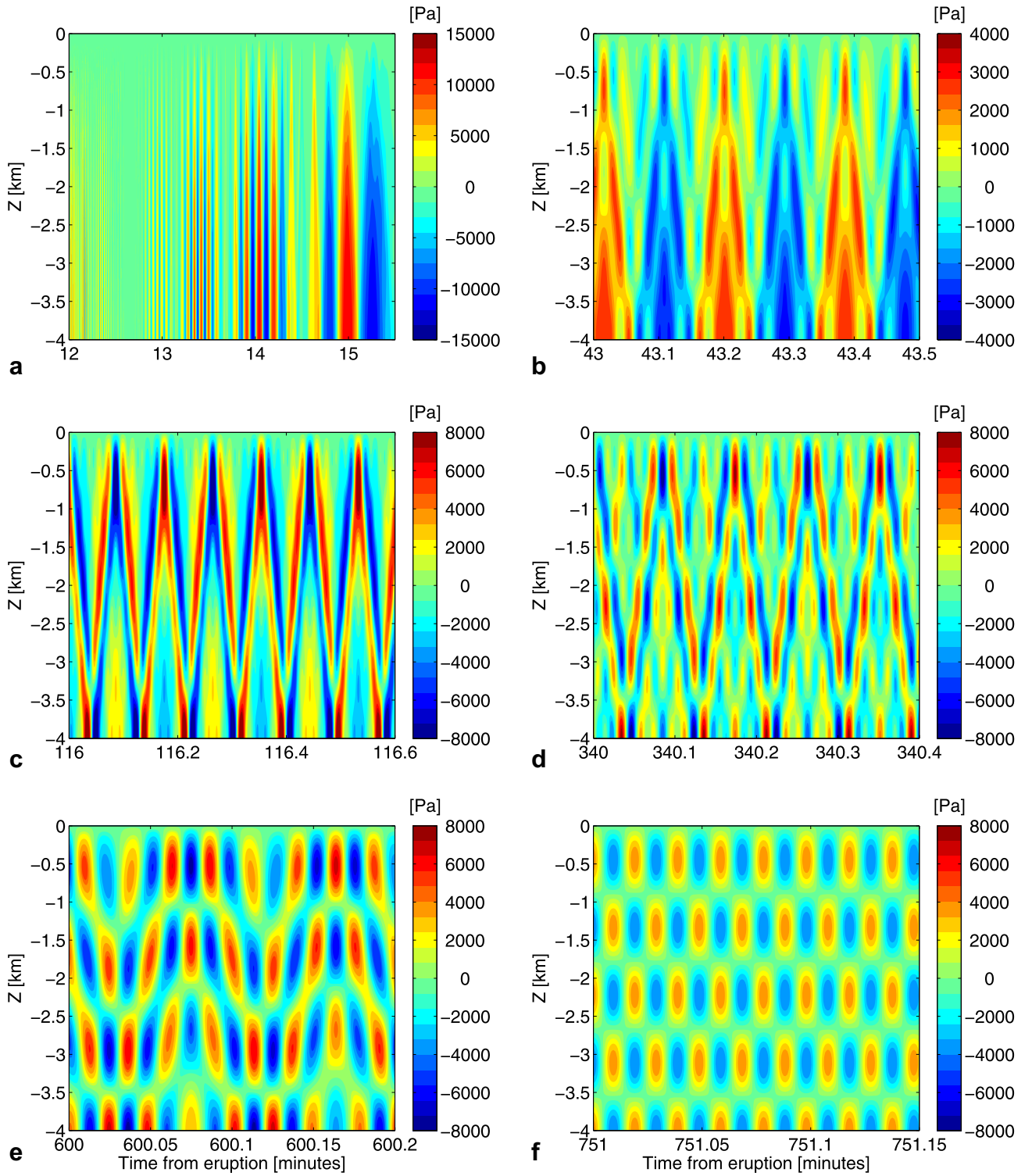


**Figure 4.** Time variation of dynamic pressure (Pa) induced by the first five AGW calculated at 1000 km from the epicenter in a 4 km deep ocean. Different temporal situations are represented corresponding to Figure 4a arrival of AGWs, (b)–(f) first to fifth mode as leading mode. Comparable maximum (in red) and minimum (in blue) pressure values can be observed from 1 to 4 km water depth at the arrival of the AGW. The simulation considers vertical and lateral extents of bottom motion of 1 m and 40 km, respectively; the water density ($\rho = 1000$ kg/m$^3$) and speed of sound ($c = 1500$ m/s) are constants.

and slow slip episodes. For different representative water depths, the evanescent time of the first AGW increases with distance to the epicenter and the duration of the bottom uplift, while decreases with the water depth.

Practically, the proposed analysis can assist in the implementation of an AGW early tsunami detection system, starting from applying the appropriate earthquake models, to identifying the relevant measurement equipment and their optimal locations. These detection systems should work accurately based on the analysis of the first AGW mode. It must be noted that the first AGW mode, for water depths from about 1000 to 7000 m, has a long wavelength that cannot be trapped within the underwater sound channel (SOFAR), while under certain conditions higher modes could be trapped. The duration of the bottom uplift can be obtained both by the analysis of (i) the evolution of AGW frequency, and by (ii) the time that take the first mode to become evanescent. On the other hand, the magnitude of the bottom uplift displacement can be estimated from the magnitude of the dynamic pressure variation. To this end, broadband pressure sensors, hydrophones, or seismometers should be capable of measuring pressure variations $O(10^4)$ Pa. Minimum sampling rates of 40–50 Hz should be used in order to measure the first and higher AGW modes.

The induced pressure field spans the entire depth and some nodes of zero pressure could exist in the absence of the first mode. While the optimal depth in terms of pressure magnitude can be at various depths, from technical considerations it is more practical to have the sensors close to the bottom yet far enough to avoid topographic effects.

The frequency of the first AGW typically varies between 0.094 and 0.375 Hz for an epicenter at 7 and 1 km water depths, respectively. If the fifth mode is analyzed, frequencies between 0.482 and 3.375 Hz are to be expected. It must be noticed that deep ocean sea state noise might mask the detection of AGW in the band 0.05–0.7 Hz [e.g., *Wilson et al*., 2003; *Gualtieri et al*., 2015; *Tian and Ritzwoller*, 2015].

This study neglects the effects of energy dissipation by bottom friction, energy scattering by bottom irregularities, energy scattering by three-dimensional effects and coupling of AGWs to the elastic ocean bottom. All these effects may act to reduce the dynamic pressure variations induced by AGW far from the epicenter. However, AGWs can travel a distance of $O(10^3)$ km with a negligible damping [*Bolshakova et al*., 2011; *Kadri and Stiassnie*, 2012]

Despite the recent advances in the theoretical understanding of AGWs, it is essential to address the link between the detection of AGWs and the actual generation of a conspicuous tsunami in future work based on field data analysis.

## Appendix A: AGWs From Submarine Earthquakes

*Stiassnie* [2010] derived an analytical expression for the wave radiation by a vertical bottom displacement, $\zeta_0$, for the case of a rigid constant seabed. Using the method of stationary phase, the free surface evolution, $\eta$, and the dynamic bottom pressure, $P_b$, of AGWs generated by a submarine earthquake in the far field ($x/h \gg 1$) can be obtained by:

$$\hat{\eta}=\frac{\eta}{\zeta_0}=\sum_{n=1}^{\infty}\frac{(-1)2^{5/2}\hat{t}^{1/2}}{\sqrt{\pi}\alpha_n^{5/2}\hat{c}^{1/2}\hat{\tau}\hat{x}}[1-(\hat{x}/\hat{c}\hat{t})^2]^{5/4}A \tag{A1}$$

$$\hat{P}_b=\frac{P_b}{\rho g\zeta_0}=\sum_{n=1}^{\infty}\frac{2^{5/2}\hat{t}^{1/2}\hat{c}^{3/2}}{\sqrt{\pi}\alpha_n^{3/2}\hat{\tau}\hat{x}}[1-(\hat{x}/\hat{c}\hat{t})^2]^{1/4}A \tag{A2}$$

where

$$A=\sin\left[\frac{\alpha_n\hat{c}\hat{\tau}/2}{\sqrt{1-(\hat{x}/\hat{c}\hat{t})^2)}}\right]\sin\left[\frac{\alpha_n\hat{b}\hat{x}/(\hat{c}\hat{t})}{\sqrt{1-(\hat{x}/\hat{c}\hat{t})^2)}}\right]\cos\left[\alpha_n(\hat{c}^2\hat{t}^2-\hat{x}^2)^{1/2}+\frac{\pi}{4}\right] \tag{A3}$$

and $\alpha_n=(2n-1)\pi/2$. Equations (A1) and (A2) are valid for any $\hat{t}\geq\hat{x}/\hat{c}$ and all variables are made dimensionless, according to:

$$\hat{x}=x/h,\quad \hat{b}=b/h,\quad \hat{t}=\tilde{t}-0.5\hat{\tau},\quad \tilde{t}=t\sqrt{g/h},\quad \hat{\tau}=\tau\sqrt{g/h},\quad \hat{c}=c/\sqrt{gh} \tag{A4}$$

where $2b$ is the lateral extents of the bottom motion, $x$ is the distance between the epicenter and the analyzed point, and $\tau$ is the duration of bottom motion.

According to *Stiassnie* [2010], the frequency of AGW generated by a bottom uplift presents an exponential decay behavior over time given by

$$\hat{\omega}_n = \omega_n h^{1/2}/g^{1/2} = \frac{\alpha_n \hat{c}}{\sqrt{1-(\hat{x}/\hat{c}\hat{t})^2}} \tag{A5}$$

Thus the dispersion relation (1) must be solved for each time $t$ and position $x$. Since the wavenumber $k_n$ depends on relation (2) an AGW mode generated by a bottom uplift becomes evanescent at a critical time when $k_n$ becomes imaginary, i.e., an AGW mode becomes evanescent when $k_n \leq \mu_n$.

**Acknowledgments**
The first author acknowledges the Postdoctoral Scholar Program at the Woods Hole Oceanographic Institution, with funding provided by the University of Haifa. Request for access to the data presented in this paper can be sent to toliveira@whoi.edu.

## References

Abdolali, A., C. Cecioni, G. Bellotti, and J. Kirby (2015a), Hydro-acoustic and tsunami waves generated by the 2012 Haida Gwaii earthquake: Modeling and in situ measurements, *J. Geophys. Res. Oceans*, *120*, 958–971, doi:10.1002/2014JC010385.

Abdolali, A., J. T. Kirby, and G. Bellotti (2015b), Depth-integrated equation for hydro-acoustic waves with bottom damping, *J. Fluid Mech.*, *766*, R1, doi:10.1017/jfm.2015.37.

Ammon, C. J., et al. (2005), Rupture process of the 2004 Sumatra-Andaman earthquake, *Science*, *308*, 1133–1139, doi:10.1126/science.1112260.

Banerjee, P., F. F. Pollitz, and R. Brgmann (2005), The size and duration of the Sumatra-Andaman earthquake from far-field static offsets, *Science*, *308*, 1769–1772, doi:10.1126/science.1113746.

Bolshakova, A., S. Inoue, S. Kolesov, H. Matsumoto, M. Nosov, and T. Ohmachi (2011), Hydroacoustic effects in the 2003 Tokachi-oki tsunami source, *Russ. J. Earth Sci.*, *12*, ES2005, doi:10.2205/2011ES000509.

Cecioni, C., G. Bellotti, A. Romano, A. Abdolali, P. Sammarco, and L. Franco (2014), Tsunami early warning system based on real-time measurements of hydro-acoustic waves, *Proc. Eng.*, *70*, 311–320, doi:10.1016/j.proeng.2014.02.035.

Chierici, F., L. Pignagnoli, and D. Embriaco (2010), Modeling of the hydroacoustic signal and tsunami wave generated by seafloor motion including a porous seabed, *J. Geophys. Res.*, *115*, C03015, doi:10.1029/2009JC005522.

de Groot-Hedlin, C. D. (2005), Estimation of the rupture length and velocity of the Great Sumatra earthquake of Dec 26, 2004 using hydroacoustic signals, *Geophys. Res. Lett.*, *32*, L11303, doi:10.1029/2005GL022695.

Eyov, E., A. Klar, U. Kadri, and M. Stiassnie (2013), Progressive waves in a compressible-ocean with an elastic bottom, *Wave Motion*, *50*, 929–939, doi:10.1016/j.wavemoti.2013.03.003.

Farrell, W. E., and W. Munk (2010), Booms and busts in the deep, *J. Phys. Oceanogr.*, *40*, 2159–2169, doi:10.1175/2010JPO4440.1.

Grilli, S. T., M. Asce, M. Ioualalen, J. Asavanant, F. Shi, J. T. Kirby, and P. Watts (2008), Source constraints and model simulation of the December 26, 2004, Indian Ocean Tsunami, *J. Waterw. Port Coastal Ocean Eng.*, *133*, 414–428.

Gualtieri, L., E. Stutzmann, Y. Capdeville, V. Farra, A. Mangeney, and A. Morelli (2015), On the shaping factors of the secondary microseismic wavefield, *J. Geophys. Res.*, *120*, 6241–6262, doi:10.1002/2015JB012157.

Heki, K., Y. Otsuka, N. Choosakul, N. Hemmakorn, T. Komolmis, and T. Maruyama (2006), Detection of ruptures of Andaman fault segments in the 2004 great Sumatra earthquake with coseismic ionospheric disturbances, *J. Geophys. Res.*, *111*, B09313, doi:10.1029/2005JB004202.

Hendin, G., and M. Stiassnie (2013), Tsunami and acoustic-gravity waves in water of constant depth, *Phys. Fluids*, *25*(8), 086103, doi:10.1063/1.4817996.

Kadri, U. (2014), Deep ocean water transport by acoustic-gravity waves, *J. Geophys. Res. Oceans*, *119*, 7925–7930, doi:10.1002/2014JC010234.

Kadri, U. (2015), Wave motion in a heavy compressible fluid: Revisited, *Eur. J. Mech., Part B*, *49*, 50–57, doi:10.1016/j.euromechflu.2014.07.008.

Kadri, U. (2016a), Triad resonance between a surface-gravity wave and two high frequency hydro-acoustic waves, *Eur. J. Mech., Part B*, *55*, 157–161, doi:10.1016/j.euromechflu.2015.09.008.

Kadri, U. (2016b), Generation of hydroacoustic waves by an oscillating ice block in arctic zones, *Adv. Acoust. Vib.*, *2016*, 8076108.

Kadri, U., and M. Stiassnie (2012), Acoustic-gravity waves interacting with the shelf break, *J. Geophys. Res.*, *117*, C03035, doi:10.1029/2011JC007674.

Kadri, U., and M. Stiassnie (2013), Generation of an acoustic-gravity wave by two gravity waves, and their subsequent mutual interaction, *J. Fluid Mech.*, *735*, R6, doi:10.1017/jfm.2013.539.

Kadri, U., and T. R. Akylas (2016), On resonant triad interactions of acoustic-gravity waves, *J. Fluid Mech.*, *788*, R1, doi:10.1017/jfm.2015.721.

Kanamori, H. (2006), Seismological aspects of the December 2004 Great Sumatra-Andaman Earthquake, *Earthquake Spectra*, *22*, 1–12, doi:10.1193/1.2201969.

Kibblewhite, A. C., and K. C. Ewans (1985), Wavewave interactions, microseisms, and infrasonic ambient noise in the ocean, *J. Acoust. Soc. Am.*, *78*, 981–994.

Kozdon, J. E., and E. M. Dunham (2014), Constraining shallow slip and tsunami excitation in megathrust ruptures using seismic and ocean acoustic waves recorded on ocean-bottom sensor networks, *Earth Planet. Sci. Lett.*, *396*, 56–65, doi:10.1016/j.epsl.2014.04.001.

Longuet-Higgins, M. S. (1950), A theory of the origin of microseisms, *Philos. Trans. R. Soc. London A*, *243*, 1–35.

Maeda, T., and T. Furumura (2013), FDM simulation of seismic waves, ocean acoustic waves, and tsunamis based on tsunami-coupled equations of motion, *Pure Appl. Geophys.*, *170*, 109–127, doi:10.1007/s00024-011-0430-z.

Miyoshi, H. (1954), Generation of the tsunami in compressible water (Part I), *J. Oceanogr. Soc. Jpn.*, *10*, 1–9.

Nosov, M. A. (1999), Tsunami generation in compressible ocean, *Phys. Chem. Earth, Part B*, *24*, 437–441, doi:10.1016/S1464-1909(99)00025-8.

Nosov, M. A., and S. V. Kolesov (2007), Elastic oscillations of water column in the 2003 Tokachi-Oki tsunami source: In-situ measurements and 3-d numerical modelling, *Nat. Hazards Earth Syst. Sci.*, *7*, 243–249, doi:10.5194/nhess-15-627-201500025-8.

Pietrzak, J., A. Socquet, D. Ham, W. Simons, C. Vigny, R. J. Labeur, E. Schrama, G. Stelling, and D. Vatvani (2007), Defining the source region of the Indian Ocean Tsunami from GPS, altimeters, tide gauges and tsunami models, *Earth Planet. Sci. Lett.*, *261*, 49–64, doi:10.1016/j.epsl.2007.06.002.

Renzi, E., and F. Dias (2014), Hydro-acoustic precursors of gravity waves generated by surface pressure disturbances localised in space and time, *J. Fluid Mech.*, *754*, 250–262, doi:10.1017/jfm.2014.398.

Sammarco, P., C. Cecioni, G. Bellotti, and A. Abdolali (2013), Depth-integrated equation for large-scale modelling of low-frequency hydroacoustic waves, *J. Fluid Mech.*, *722*, R6, doi:10.1017/jfm.2013.153.

Stiassnie, M. (2010), Tsunamis and acoustic-gravity waves from underwater earthquakes, *J. Eng. Math.*, *67*, 23–32, doi:10.1007/s10665-009-9323-x.

Synolakis, C. E., J.-P. Bardet, J. C. Borrero, H. L. Davies, E. A. Okal, E. A. Silver, S. Sweet, and D. R. Tappin (2002), The slump origin of the 1998 Papua New Guinea Tsunami, *Proc. R. Soc. London, Ser. A*, *458*, 763–789.

Tian, Y., and M. H. Ritzwoller (2015), Directionality of ambient noise on the Juan de Fuca plate: Implications for source locations of the primary and secondary microseisms, *Geophys. J. Int.*, *201*(1), 429–443, doi:10.1093/gji/ggv024.

Wilson, D. K., G. V. Frisk, T. E. Lindstrom, and C. J. Sellers (2003), Measurement and prediction of ultralow frequency ocean ambient noise off the eastern U.S. coast, *J. Acoust. Soc. Am.*, *113*, 3117–3133, doi:10.1121/1.1568941.

Yamamoto, T. (1982), Gravity waves and acoustic waves generated by submarine earthquakes, *Int. J. Soil Dyn. Earthquake Eng.*, *1*, 75–82, doi:10.1016/0261-7277(82)90016-X.